ACS OMEGA

http://pubs.acs.org/journal/acsodf

Article

Different Phenomena in Magnetic/Electrical Properties of Co(II) and Ni(II) Isomorphous MOFs

Shi-Fen Li,[§] Quan Wang,[§] Ye-Ping Li, Xiao Geng, LiJia Zhao, Mei He, Lin Du,* and Qi-Hua Zhao*

Cite This: *ACS Omega* 2021, 6, 9213–9221

Read Online

ACCESS | Metrics & More | Article Recommendations | Supporting Information

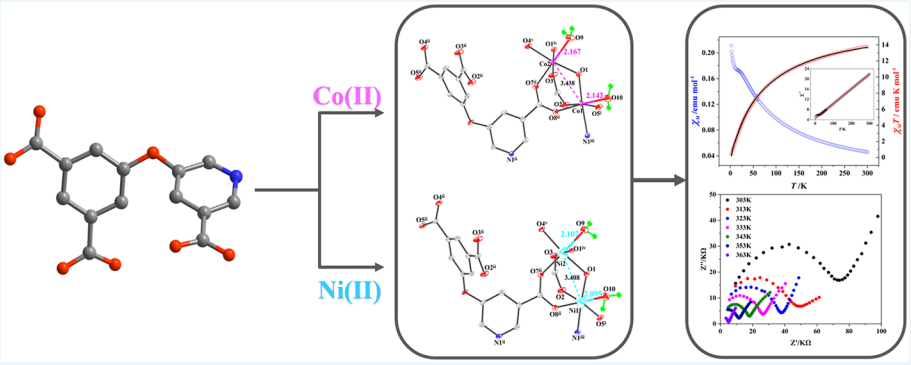

ABSTRACT: Two unprecedented and stable metal−organic frameworks, $\{[Co_2(H_2O)_2(L)(OH)]\cdot 2.5H_2O\cdot 0.5DMF\}_n$ (**1**) and $\{[Ni_2(H_2O)_2(L)(OH)]\cdot 1.75H_2O\}_n$ (**2**), have been synthesized (H_3L = 5-(5-carboxy-pyridin-3-yloxy)-isophthalic acid, DMF = *N*,*N*-dimethylformamide). Structural analysis shows that **1** and **2** are heteronuclear isomorphous, possessing a three-dimensional (3D) (4,8)-connected flu/fluorite topological framework formed through the interconnection of tetranuclear butterfly $\{M_4(COO)_6(OH)_2\}$ clusters and the ligands. Although the frameworks of these two compounds are similar, their magnetic properties are different. Compound **1** exhibits an antiferromagnetic interaction in the high-temperature region, while **2** shows a weak ferromagnetic interaction in the whole-temperature region. Furthermore, considering the presence of hydroxyl groups and water molecules in the frameworks, we tested their proton conductivity. The efficient proton transfer pathway in the framework endowed **1** and **2** with excellent proton conductivities of 9.07×10^{-5} and 1.29×10^{-4} S·cm^{-1} at 363 K and 98% relative humidity (RH), respectively.

INTRODUCTION

Metal−organic frameworks (MOFs) have attracted much attention as a functional material in recent years. This is not only because of their intriguing structures but also because of their potential applications in the fields of luminescence, catalysis, adsorption, proton conduction, and so on.[1−6] In particular, MOFs are excellent candidates to study the elusive magnetostructural correlations and some fundamental magnetic phenomena, such as spin-canting, spin-frustration, metamagnetism, single-molecule magnets, and so on.[7−11]

In the process of constructing interesting magnetic materials, the selection of different spin states and anisotropic spins of the paramagnetic metal ions plays a very important role. The metal center can exist in multiple electronic states, variable oxidation states, and changeable coordination numbers, so it can form a variety of magnetic centers to regulate the interesting magnetic behavior of MOFs. Ma et al. obtained three isomorphous compounds, formulated as $[M_2(bcpe)(N_3)_4]\cdot H_2O$ (bcpe = 1,2-bis(*N*-carboxymethyl-4-pyridinio)ethane, M = Mn, Co, and Ni). The anionic uniform M(II) chains with mixed (syn-syn-COO)(EO-N_3)$_2$ triple bridges are cross-linked by the cationic bis(pyridinium) spacers to generate 2D coordination layers. Because the magnetic change in the $M(COO)(N_3)_2$ series may be related to the different $t_{2g}^x e_g^y$ configurations of the metal ions in the octahedral geometry, triple bridges mediate antiferromagnetic coupling in the Mn(II) compound but ferromagnetic coupling in the Co(II) and Ni(II) species.[12] Zhang et al. synthesized two new isomorphous metal−organic frameworks with a porous (10,3)-a network, namely, as $(H_2NMe_2)[M(tzdc)]\cdot 0.5H_2O$ ($tzdc^{3-}$ = 1,2,3-triazole-4,5-dicarboxylate, M = Mn and Co). The triangular arrangement of paramagnetic metal centers in the frameworks makes them exhibit geometrically frustrated magnetism. Particularly, distinct spin-glassy behavior is observed below 2.4 K in the Co(II) compound owing to the

Received: January 31, 2021
Accepted: March 16, 2021
Published: March 26, 2021

© 2021 The Authors. Published by American Chemical Society

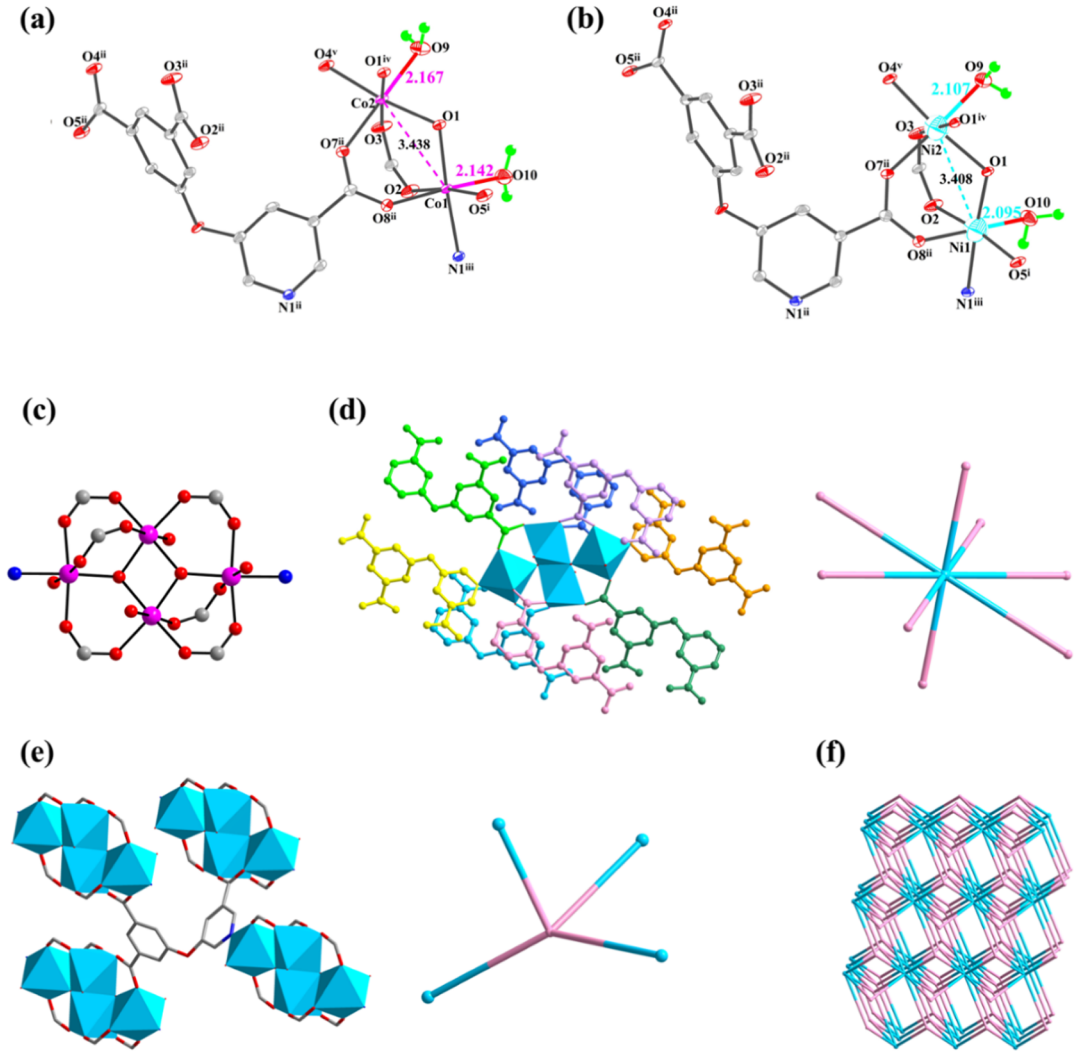

Figure 1. (a) Coordination environment of **1** at 30% probability level (symmetry codes: (i) $x, y + 1, z$; (ii) $x + 1, y, z$; (iii) $-x + 1, -y + 2, -z$; (iv) $-x + 2, -y + 2, -z + 1$; (v) $-x + 2, -y + 1, -z + 1$; red: O; blue: N; gray: C; pink: Co). (b) Coordination environment of **2** at the 30% probability level (symmetry codes: (i) $x, y + 1, z$; (ii) $x + 1, y, z$; (iii) $-x + 1, -y + 2, -z$; (iv) $-x + 2, -y + 2, -z + 1$; (v) $-x + 2, -y + 1, -z + 1$; red: O; blue: N; gray: C; turquoise: Ni). (c) Tetranuclear cluster formed in **1**. (d) Schematic illustrating that the tetranuclear SBU can be reduced to an eight-connected node. (e) Scheme illustrating that the L^{3-} can be reduced to a four-connected node. (f) Schematic representation of the (4,8)-connected flu/fluorite-topology framework.

remarkable magnetic anisotropy of Co(II) ions and the stronger antiferromagnetic interaction compared to the Mn(II) compounds, which have no obvious long-range magnetic ordering and/or spin−glass behavior observed down to 2.0 K.[13]

In addition, organic ligands are another essential factor for the construction of magnetic MOFs.[14] The magnetic properties can be well adjusted by modifying suitable functional organic ligands, which affect the magnetic exchange pathways of the metal centers. The polycarboxylate ligands attract the attention of researchers in the assembly of magnetic MOFs not only due to their variable coordination modes but also due to their ability of magnetic exchange with paramagnetic metal centers.[15] A large number of MOFs with different dimensions and various topologies based on polycarboxylate ligands have been reported in the literature.[16,17] The diversity of these materials provides a wonderful opportunity to further understand the basic magnetic phenomenon. Furthermore, the polycarboxylate ligands can easily form multinuclear cluster units with paramagnetic metal centers. Zhu et al. obtained a compound exhibiting antiferromagnetic interaction, which connected network formed through the interconnection of the tetranuclear Cu(II) clusters and the polycarboxylate ligand.[18] Liu et al. synthesized a trinuclear Ni(II) complex, which reveals that weak antiferromagnetic interactions occur between the bridging trinuclear Ni(II) ions.[19] In this work, we choose 5-(5-carboxy-pyridin-3-yloxy)-isophthalic acid (H_3L) as the ligand to construct magnetic MOFs, which is a nitrogen heterocyclic tricarboxylic acid with a semirigid structure. The introduction of nitrogen heterocycles into ligands may bring more coordination modes and construct higher-dimensional frameworks, which may lead to enhanced magnetic interactions.[20] At the same time, the semirigidity of the ligand may also form a rare framework or even a novel topology.[21] Furthermore, this ligand has not been fully studied.

Fortunately, we successfully obtained two new MOFs based on H_3L for the first time, formulated as $\{[Co_2(H_2O)_2(L)(OH)]\cdot 2.5H_2O\cdot 0.5DMF\}_n$ (**1**) (DMF = *N*,*N*-dimethylformamide) and $\{[Ni_2(H_2O)_2(L)(OH)]\cdot 1.75H_2O\}_n$ (**2**), which exhibit different magnetic interactions. MOFs based on nitrogen heterocyclic polycarboxylic acid ligands also have excellent

https://doi.org/10.1021/acsomega.1c00574
ACS Omega 2021, 6, 9213−9221

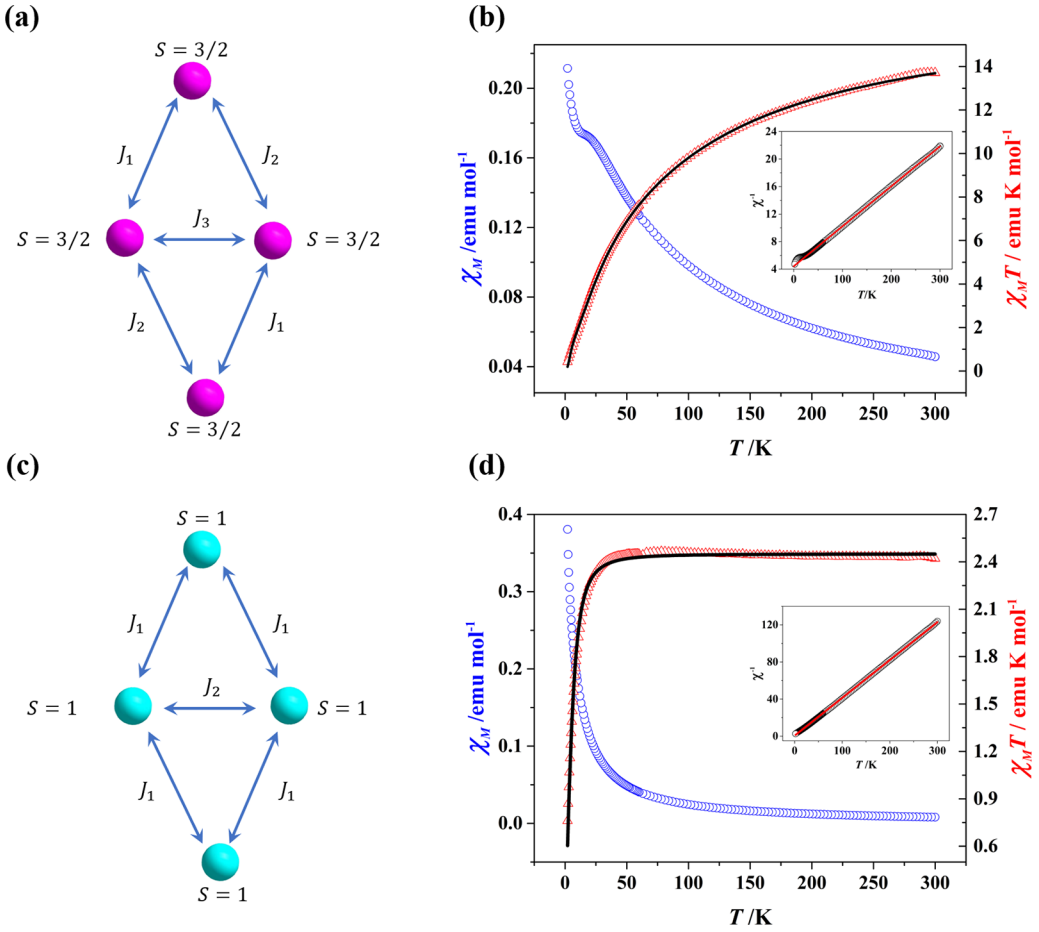

Figure 2. (a) Molecular symmetry of **1**. (b) Magnetic data of **1**. (c) Molecular symmetry of **2**. (d) Magnetic data of **2** (include χ_M^{-1}, $\chi_M T$, and χ_M versus T data). Furthermore, the best fit of $\chi_M T$ product and χ_M^{-1} are all shown by a black line.

performance in the field of proton conduction.[22−25] The difference in coordination ability of nitrogen and oxygen atoms may result in incompletely coordinated carboxylic acid groups in the obtained MOFs, which is helpful to construct proton conduction channels. The carboxylic acid groups in these two MOFs we obtained are all coordinated; however, considering the presence of hydroxyl groups and water molecules in the frameworks, which can establish proton conduction channels to help proton migration, we have studied their proton conduction performance and further explored the conduction mechanism. The best proton conductivities of **1** and **2** under 363 K and 98% relative humidity (RH) are 9.07×10^{-5} and 1.29×10^{-4} S·cm^{-1}, respectively. In addition, the strength of the hydrogen-bond interaction of **1** and **2** was compared by the Hirshfeld surface analysis and the PLATON calculation.

RESULTS AND DISCUSSION

Crystal Structure. The result of single-crystal X-ray crystallographic analysis reveals that **1** and **2** belong to the triclinic system and the $P\bar{1}$ space group. Their metal coordination environment, second-building units (SBUs), and the frame structure are similar, so we take **1** as an example. The asymmetric unit of **1** includes two Co(II) ions, one completely deprotonated L^{3-} anion, two coordination water molecules, one μ_3-OH, two and one-half crystalline water molecules, and half guest DMF molecule (Figure 1a). All Co(II) atoms have distorted octahedral geometry. Co1 is surrounded by three oxygen atoms from different carboxylate groups, one nitrogen atom from L^{3-} ligand, one coordinated water molecule, and one μ_3-OH (Co1−O distances range from 2.019(2) to 2.163(2) Å, Co1−N1 distance is 2.152(3) Å). Co2 is surrounded by three oxygen atoms from different carboxylate groups, one coordinated water molecule, and two μ_3-OH (Co2−O distances range from 2.047(2) to 2.168(3) Å). Each L^{3-} is linked to seven Co(II) ions by three bidentate bridged carboxyl groups and one pyridine group (Figure S1). Four symmetry-related Co(II) atoms were connected via μ_3-OH groups to form a $[Co_4(\mu_3\text{-}OH)_2]^{6+}$ cluster subunit. Such a cluster is held together by six carboxylate groups, thereby constituting the tetranuclear butterfly-shaped $[Co_4(\mu_3\text{-}OH)_2(COO)_6]$ cluster (Figure 1c). In the tetranuclear clusters, four Co(II) ions are totally coplanar with the Co···Co distances of 3.438 Å (Co1···Co2). The tetranuclear clusters are connected with 12 identical adjacent clusters by eight μ_7-κ^7O:O′:O″:O‴:O⁗:O⁗′:N−L^{3-} to form a three-dimensional (3D) framework.

The application of the topological approach is beneficial for us to better understand this complicated framework. Each SBU can be simplified as an eight-connection node, while a L^{3-} ion can be defined as a four-connection node connecting four adjacent SBUs (Figure 1d,e). Therefore, the structure of **1** is a (4,8)-connected flu/fluorite topological framework with the Schläfli symbol of $\{4^{12}\cdot6^{12}\cdot8^4\}\{4^6\}_2$ (Figure 1f).

Although compounds **1** and **2** are heteronuclear isomorphous, there are still some differences in the bond lengths of coordinated water ($M-O_{water}$), which lead to their different properties. The bond lengths of Co1−O10, Co2−O9, Ni1−

https://doi.org/10.1021/acsomega.1c00574
ACS Omega 2021, 6, 9213−9221

O10, and Ni2−O9 are 2.142, 2.167, 2.095, and 2.107 Å, respectively (Figure 1a,b). From the data, it can be found that there is a certain difference between the length of the Co−O_{water} bond and the length of the Ni−O_{water} bond. The bond length of Co−O_{water} are slightly longer than that of Ni−O_{water}.

General Characterization. The powder X-ray diffraction (PXRD), infrared spectroscopy (IR), and thermogravimetric analysis (TGA) of the two compounds have been studied before using them for experiments. The PXRD patterns of synthesized **1** and **2** are matched well with the simulated data obtained from single-crystal X-ray diffraction (Figure S2), indicating the high purity of the synthesized samples, and it is also confirmed that **1** and **2** are heteronuclear and isomorphous. The bands at 1628−1573 cm^{-1} in the IR spectrum can be assigned to the antisymmetric stretching of the $-COO^-$ groups, which indicates that all of the carboxyl groups coordinated with metal ions successfully (Figure S3). Thermogravimetric analysis proves that **1** and **2** have high thermal stability (Figure S4). For **1**, a period of sustained weight loss in the range of 0−250 °C may be caused by the successive loss of two and a half lattice water molecules, two coordinated water molecules, and a half DMF guest molecule (obsd 20.16%, calcd 21.26%). In the range of 250−450 °C, the thermogravimetric curve shows a plateau, and the crystal structure remains stable. The structure collapsed after 450 °C. The guest molecules in the two compounds are slightly different, but they show similar thermal behavior. This may be caused by the different dryness of the samples used for the thermogravimetric test.

Magnetic Properties. Considering the tetranuclear metal clusters in the structures of **1** and **2**, the magnetic susceptibility χ_M was investigated. For **1**, its $\chi_M T$ value at room temperature is 13.7 $cm^3\ Kmol^{-1}$, which is higher than the theoretical $\chi_M T$ value of 7.50 $cm^3\ Kmol^{-1}$.[26] There may be two reasons for the high χ_M value at room temperature. First, the g = 2.0 assumes that the $\chi_M T$ value is theoretical. In fact, the true g value is 2.11, which is higher than the theoretical one. Second, the Co2(II) forms an axially elongated octahedral ligand field (Figure 2a). As a result, the unquenched orbital angular momentum plays a key role in the magnetic properties of **1**. For an S = 3/2 Co^{II} ion in the $3d^7$ electron configuration with a nonzero orbital, it contributes to the magnetic moment (Figure 2b).[26,27] The χ_M^{-1} versus T data can be fitted by the Curie−Weiss law [$\chi_M = C/(T-\theta)$] from 30 to 300 K giving C = 17.44 cm^{-3} K mol^{-1} and θ = −79.54 K. Compared with the C value with the only spin, the C value is large, indicating the significant contribution of the orbital momentum. A large negative value of θ indicates that there is an overall antiferromagnetic coupling in addition to the single-ion spin−orbit coupling. The small $\chi_M T$ at low temperatures further confirms the antiferromagnetic interaction.

For **2**, as clusters **1** and **2** both crystallize in the same space group, the Ni2(II) formed an octahedral ligand field. The χ_M^{-1} versus T data can be fitted with C = 2.45 cm^{-3} K mol^{-1} and θ = −1.31 K. The magnetic behavior in the high temperature region shows the dominant ferromagnetic interactions. However, with the zero-field splitting, the $\chi_M T$ of $_4$ clusters (Figure 2c) decreased slightly at low temperatures.[28,29] Furthermore, below 35 K, the product $\chi_M T$ gradually decreases and finally reaches a value of almost zero at 2 K (Figure 2d), which indicates a weak intercluster antiferromagnetic interaction or anisotropic effects at low temperature.

To further investigate the interactions in two tetraclusters, for which a maximum was observed in the susceptibility at whole temperatures, simulations using PHI software were formed.[30] An examination of the molecular symmetry between the metal centers in **1** and **2** for magnetostructural correlations revealed an obvious trend based on the structural parameter.[31] For **1**, to fully describe the magnetic exchange between the closest Co(II) ions, three J parameters are required: two for covalent bridging motifs [Co1(μ-OCO)$_2$(μ-OH)Co2] and [Co2(μ-OH)$_2$Co2], and one for hydrogen-bonding bridging motifs [Co1(μ-OCO) (μ-O-H···O)Co2]. Furthermore, the best sets of parameters, such as the Landé factor, obtained using the model are needed to account for the influence of single-site factors on magnetic behaviors. At present, there is no reliable model to quantitatively analyze the magnetic exchange in this complex system.[32]

For **2**, applying the van Vleck equation[33,34] to Kambe's vector coupling scheme,[35] we can obtain an analytical expression of the magnetic susceptibility from the following spin Hamiltonian

$$H = -2J_1 S_1 S_2 - 2J_2 \left[\sum_{i=1,2} S_i S_3 + S_i S_4 \right]$$

It is quite clear that deviations occur between the construction of two compounds, which might originate from two assumptions that have been made. Namely, the Ni2(II) has ferromagnetic coupling with the presence of zero-field splitting (ZFS). Considering the intercluster interactions, these magnetic couplings have been treated in a mean-field approximation, which from the following equation[36,37]

$$\chi_{tetramer} = \frac{2Ng^2\beta^2}{kT}(30e^{8x+4y} + 14e^{4y} + 5e^{-6x+4y} + e^{-10x+4y} + 28e^{4x} + 10e^{-2x} + 2e^{-6x} + 10e^{-2y} + 5e^{2x-4y} + e^{-2x-4y} + 2e^{-6y})/(9e^{8x+4y} + 7e^{4y} + 5e^{-6x+4y} + 3e^{-10x+4y} + e^{-12x+4y} + 14e^{4x} + 10e^{-2x} + 10e^{-6x} + 10e^{-2y} + 5e^{2x-4y} + 3e^{-2x-4y} + e^{-4x-4y} + 6e^{-6y} + e^{-8y}) \qquad (x = J_1/kT;\ y = J_2/kT)$$

$$\chi = \frac{\chi_{tetramer}}{1 - \frac{1zj'}{Ng^2\mu_B^2}\chi_{tetramer}}$$

where the best parameters are J_1/k_B = 2.01(9), J_2/k_B = 0.18(6), g = 2.10, and zJ'/k_B = −0.72(8). It is important to note that the resulting g value is very much in line with the Ni(II) compound. Magnetic interactions J_1 and J_2 are both ferromagnetic as also demonstrated by χ_M product in the high-temperature region.[38]

Proton Conduction Properties. Before studying the performance of proton conduction, water stability, and chemical stability of **1** and **2** have been tested. To determine water and chemical stability, the as-prepared solids were soaked in water at room temperature for a week, refluxed in boiling water for one day, or immersed in an aqueous solution of different pH (pH 1.0−11.0) for one day. The nearly unchanged PXRD patterns of **1** and **2** demonstrated their outstanding water stability and chemical stability (Figures S5 and S6).

The remarkable structural feature and prominent stability of **1** and **2** give us a chance to explore their proton conduction properties. The conductivity of almost all proton-conducting materials based on MOFs is closely related to humidity or temperature.[39] Therefore, impedance measurements were performed under different temperatures (303−363 K) and RH values (68−98% RH). The Nyquist plots show a typical proton conduction behavior, which shows a semicircle in the

https://doi.org/10.1021/acsomega.1c00574
ACS Omega 2021, 6, 9213−9221

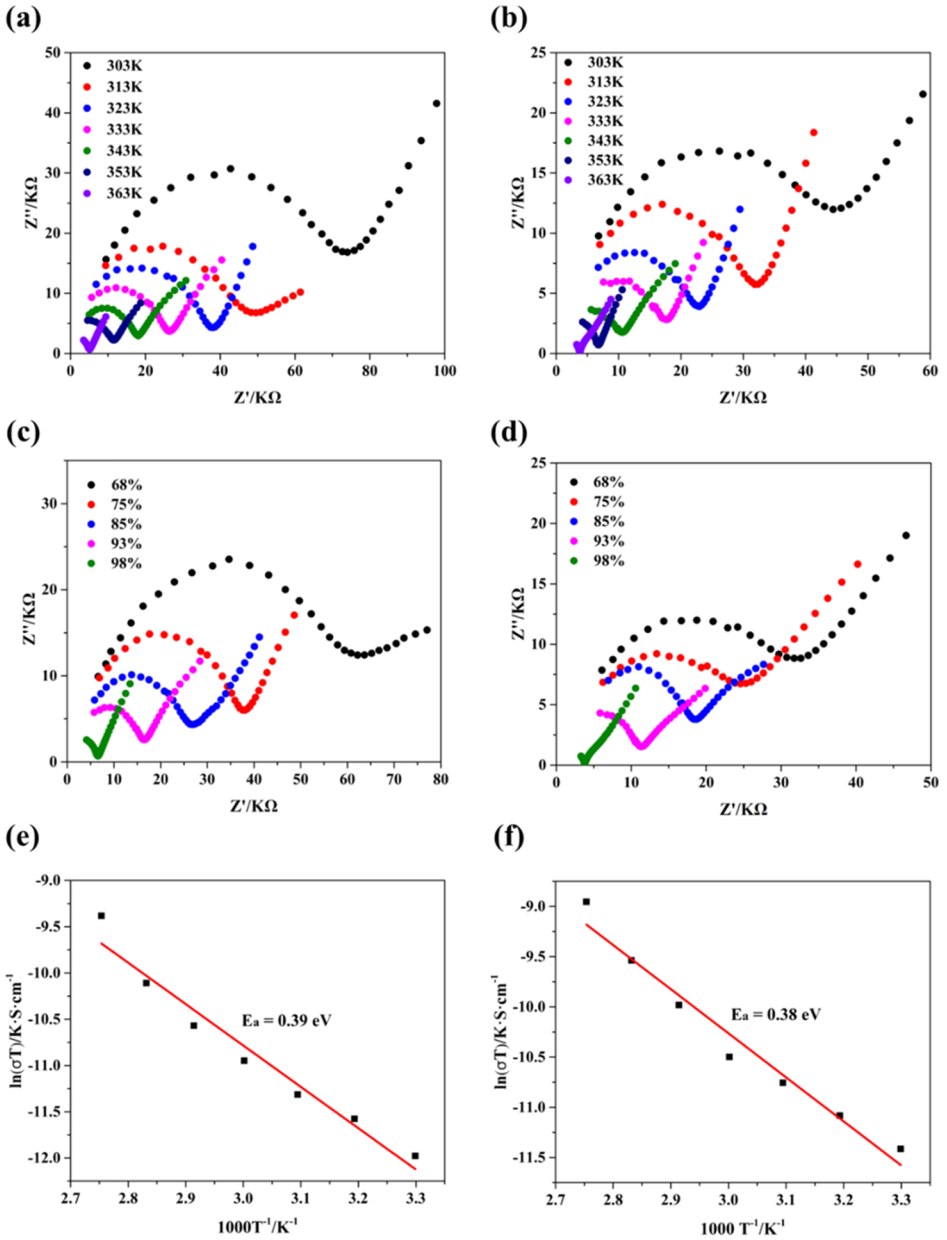

Figure 3. (a) Nyquist plots of **1** at different temperatures and 98% RH. (b) Nyquist plots of **2** at different temperatures and 98% RH. (c) Nyquist plots of **1** under different relative humidities and 363 K. (d) Nyquist plots of **2** under different relative humidities and 363 K; (e) Arrhenius plot of ln (σT) against 1000 T^{-1} of **1** under 98% RH. (f) Arrhenius plot of ln (σT) against 1000 T^{-1} of **2** under 98% RH (the red solid line represents the best fit of the data).

high-frequency region and a tail in the low-frequency region.[40] The conductivity of **1** increased significantly with the enhancement of temperature at 98% RH (Figure 3a). The obvious temperature dependence of conductivity could be attributed to the higher acidity (pK_a) of water molecules at higher temperatures.[41] Meanwhile, the temperature increase will accelerate the movement of protons, resulting in higher proton conductivity. At constant temperature (363 K), the conductivity of **1** shows a trend of growth in humidity (Figure 3c), which reveals that environmental humidity plays a key role in the construction of the proton conduction network. We performed thermogravimetric measurement for the sample after proton conduction measurements under 98% RH and 363 K (Figure S7). The TG curve of the sample after the proton conductivity measurements maintains the trend of the original sample's TG curve, which shows a higher weight loss rate. This phenomenon explains that the water content of the sample under high humidity is higher. The higher water content in the sample helps to form a richer hydrogen-bond network, thereby improving the proton conductivity.[42] With the increase in temperature and humidity, the conductivity of **2** shows a similar increasing tendency with **1** (Figure 3b,d). Their σ values under different temperatures (303−363 K) and RHs (68−98% RH) are listed in Tables S4 and S5. The best σ values of **1** and **2** under 98% RH and 363 K are 9.07×10^{-5} and 1.29×10^{-4} S·cm^{-1}, respectively. This value is comparable to the conductivity of MOFs constructed based on nitrogen-containing heterocyclic multicarboxylate ligands in other studies (Table S6).

To explore the mechanism of proton conduction, we calculated the activation energy values (E_a) according to the

https://doi.org/10.1021/acsomega.1c00574
ACS Omega 2021, 6, 9213−9221

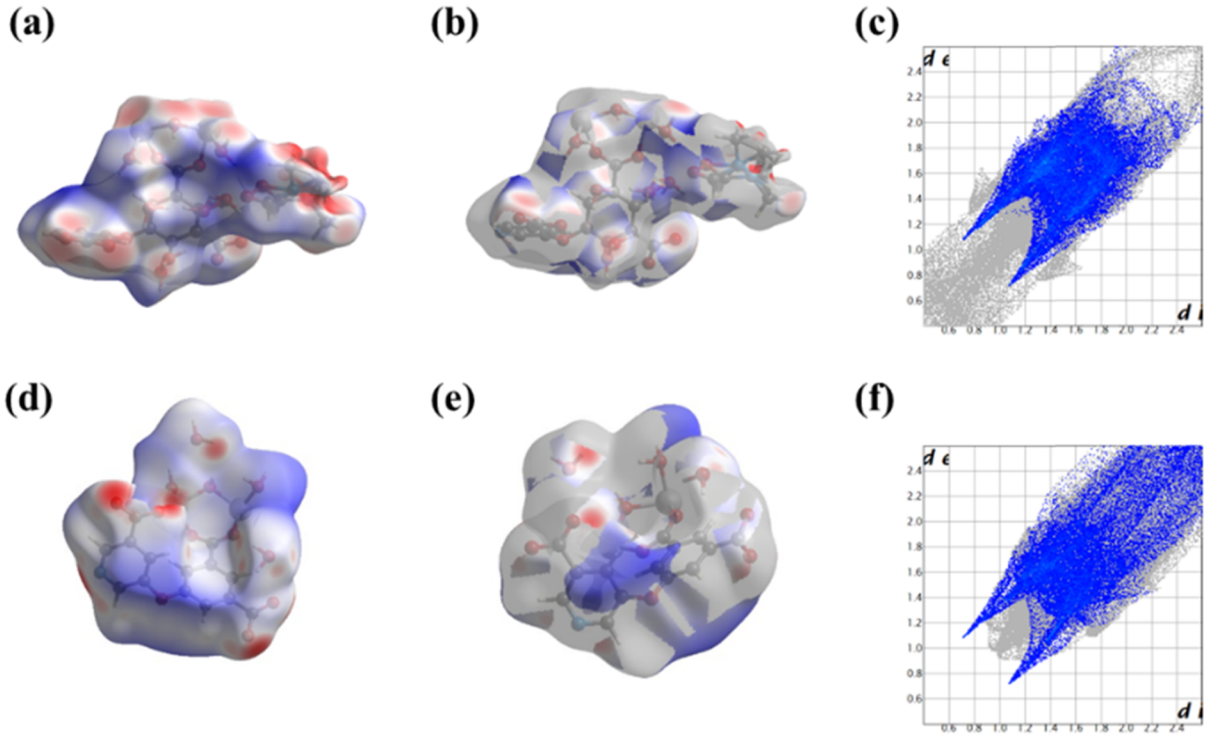

Figure 4. (a) Hirshfeld surface mapped with d_{norm} (full) of **1**. (b) Hirshfeld surface mapped with d_{norm} (O···H/H···O) of **1**. (c) Fingerprint plots (O···H/H···O) for **1**. (d) Hirshfeld surface mapped with d_{norm} (full) of **2**. (e) Hirshfeld surface mapped with d_{norm} (O···H/H···O) of **2**. (f) Fingerprint plots (O···H/H···O) for **2**.

Arrhenius equation. The E_a values under 98% RH of **1** and **2** are 0.39 and 0.38 eV, respectively, which belongs to the Grotthuss mechanism (Figure 3e,f).[43,44] This indicated that the proton conduction process is realized by the continuous formation and rearrangement of hydrogen bonds among water molecules and hydroxyl groups.[45]

The PXRD patterns of **1** and **2** after the electrochemical measurements under 98% RH and 363 K are consistent with the original ones (Figure S8), indicating that the structural rigidity of **1** and **2**. Excellent structural stability is essential for practical applications.

Hydrogen Bond Analysis. The different bond lengths of the coordinated water (M−O_{water}) may affect the interaction of hydrogen bonds in **1** and **2**. To illustrate and quantify the hydrogen-bond interactions of the crystal structures, Hirshfeld's surface analysis on all structures was carried using CrystalExplorer software. Hirshfeld surfaces mapped with d_{norm} for all of the structures of **1** and **2** are shown in Figure 4a,d. The intermolecular interaction of **1** is 98.0%, which is higher than 82.2% of **2**. O···H/H···O represents a typical hydrogen bond, and its relative contribution in **1** and **2** is 26.6 and 21.8%, respectively. The hydrogen-bond interaction sites are mainly concentrated on the oxygen atoms of carboxyl groups and water molecules on the d_{norm} surface (Figure 4b,e). The corresponding fingerprint plots show two distinct sharp spikes (Figure 4c,f).

In addition, the hydrogen bonds related to coordination water in **1** and **2** were also calculated by PLATON. According to Tables S7 and S8, it can be found that there are more hydrogen bonds involved in coordination water in **1**, and the bond lengths of **1** is relatively shorter. This all proves that the hydrogen-bond interaction in **1** is stronger than **2** due to the difference in the bond lengths of coordinated water.

CONCLUSIONS

In summary, we successfully synthesized two new dual-functional MOFs with magnetism and high proton conduction. They exhibit different magnetic properties. Compound **1** exhibits antiferromagnetic interaction in the high-temperature region, while **2** shows a weak ferromagnetic interaction in the whole-temperature region. However, there is no significant difference in their proton conductivity. The highest σ values of **1** and **2** are 9.07×10^{-5} and 1.29×10^{-4} S·cm^{-1} under 363 K and 98% RH, respectively. To the best of our knowledge, this is the first example of the investigation of proton conduction and magnetism based on MOFs assembled by H_3L. We believe that this research will provide some information for further exploration of the correlation between the structure and properties of MOFs.

EXPERIMENTAL SECTION

Materials and Methods. The ligand 5-(5-carboxy-pyridin-3-yloxy)-isophthalic acid (H_3L) was purchased from Jinan Henghua Technology Co. Ltd. All other reagents were purchased commercially and used as received without further purification. Elemental analysis was performed by an Elementar Vario ELIII instrument. The powder X-ray diffraction (PXRD) was obtained from a Rigaku X-ray diffractometer (Cu Kα, λ = 1.5418 Å). Infrared spectrum (IR) was measured in the range ν = 400−4000 cm^{-1} using KBr pellets by Thermo Scientific FTIR-Nicolet iS10. Thermogravimetric analysis (TGA) was conducted on a Metler-Toledo synchronous differential thermal analyzer under N_2 atmosphere and the test range from 25 to 800 °C at the heating rate of 10 °C min^{-1}. Magnetic susceptibility χ_M was investigated between 2 and 300 K under 1000 Oe magnetic field using a SQUID magnetometer (Quantum MPMS). The alternating current (AC) impedance spectra were measured on a

https://doi.org/10.1021/acsomega.1c00574
ACS Omega 2021, 6, 9213−9221

Metrohm Autolab Electrochemical workstation using a quasi-four-probe method (frequencies: 1 Hz to 1 MHz; ac voltage amplitude: 0.01 V).

Synthesis of {[$Co_2(H_2O)_2(L)(OH)$]·2.5H_2O·0.5DMF}$_n$ (1). H_3L (0.02 mmol, 6.1 mg), $Co(CH_3COO)_2·4H_2O$ (0.03 mmol, 7.5 mg), NaOH (0.02 mmol, 0.80 mg), 0.3 mL of DMF, and 2.0 mL of H_2O were added in a 5 mL vial. Then, the vial was kept in an autoclave at 120 °C for one day. After cooling to room temperature, pink crystals were collected and washed with deionized water several times. Yield: 63% (based on H_3L). Elemental analysis: Anal. calcd for $C_{28}H_{22}Co_4N_2O_{20}·5(H_2O)·C_3H_7NO$: C, 33.65; H, 3.53; O, 37.63; N, 3.80. Found: C, 33.75; H, 3.67; O, 37.74; N, 3.81%. Main IR data (KBr, cm^{-1}): 3423(s), 2973(w), 1628(s), 1573(s), 1437(m), 1387(s), 1307(m), 1267(m), 1151(w), 1095(w), 1049(w), 990(w), 896(w), 811(m), 782(m), 714(w), 615(w).

Synthesis of {[$Ni_2(H_2O)_2(L)(OH)$]·1.75H_2O}$_n$(2). The synthesis steps of **2** are the same as those of **1**, except the metal salt is replaced with $NiCl_2·6H_2O$ (0.03 mmol, 7.1 mg). Green crystals of **2** were obtained and washed with deionized water. Yield: 54% (based on H_3L). Elemental analysis: Anal. calcd for $C_{28}H_{22}N_2Ni_4O_{20}·3.5(H_2O)$: C, 33.45; H, 2.89; O, 37.44; N, 2.79. Found: C, 33.62; H, 2.96; O, 37.74; N, 2.91%. Main IR data (KBr, cm^{-1}): 3424(s), 2974(w), 1630(s), 1572(s), 1437(m), 1386(s), 1305(m), 1268(m), 1153(w), 1096(w), 1050(w), 898(w), 812(m), 781(m), 713(w), 613(w), 453(w).

Crystallography. Single-crystal X-ray diffraction data were collected on a Bruker Smart APEXII single-crystal diffractometer (Mo Kα, λ = 0.7101 Å). SADABS program was used to absorb and correct the crystal diffraction data.[46] The structure was solved by direct methods and refined by SHELXL software package employing full-matrix least-squares methods against F^2.[47] All nonhydrogen atoms were located in Fourier transform and anisotropy refinement. Hydrogen atoms were placed in calculated positions and refined isotropically using the riding model. The geometrical calculations were carried out using the program PLATON.[48] Details of the crystallographic data for **1** and **2** are listed in Table S1. Also, selected bond lengths (Å) as well as angles (deg) are listed in Tables S2 and S3, respectively. The CCDC numbers of 2008561 and 2054072 are for **1** and **2**, respectively.

Proton Conduction Measurements. Approximately 30 mg of crystalline powder of **1** or **2** was pressed into a wafer with a steel mold with a diameter of 0.5 cm under a pressure of 3.5 MPa for 5 min. The thickness of the wafer was measured with a vernier caliper. Then, the wafer was connected to two Cu electrodes and activated at different humidities for 24 h. The AC impedance of the sample was tested under 303−363 K and 68−98% RH. The conductivity was calculated by the equation $\sigma = L/RS$, where L, R, and S represent the thickness, the resistance, and cross-sectional area of the sample, respectively. The activation energy (E_a) was calculated by the Arrhenius formula: $\ln(\sigma T) = (\ln A - E_a)/kT$, where A and k are the pre-exponential factor and Boltzmann's constant, respectively.

■ ASSOCIATED CONTENT

Supporting Information

The Supporting Information is available free of charge at https://pubs.acs.org/doi/10.1021/acsomega.1c00574.

Coordination mode of H_3L (Figure S1), PXRD data (Figure S2), IR (Figure S3), TGA (Figure S4), stability of **1** and **2** (Figures S5, S6, and S8), TGA plots before and after the proton conductivity measurement (Figure S7), crystal data and selected bond lengths and angles (Tables S1−S3), proton conductivity (Tables S4 and S5), comparison of the proton conductivity with other proton-conducting materials (Table S6), and hydrogen-bonding data (Tables S7 and S8) (PDF)

Crystallographic data for **1** (CIF)

Crystallographic data for **2** (CIF)

■ AUTHOR INFORMATION

Corresponding Authors

Lin Du − *Key Laboratory of Medicinal Chemistry for Natural Resource, Ministry of Education; Yunnan Research & Development Center for Natural Products; School of Chemical Science and Technology, Yunnan University, Kunming 650091, P. R. China*; Email: lindu@ynu.edu.cn

Qi-Hua Zhao − *Key Laboratory of Medicinal Chemistry for Natural Resource, Ministry of Education; Yunnan Research & Development Center for Natural Products; School of Chemical Science and Technology, Yunnan University, Kunming 650091, P. R. China*; orcid.org/0000-0001-8165-1793; Email: qhzhao@ynu.edu.cn

Authors

Shi-Fen Li − *Key Laboratory of Medicinal Chemistry for Natural Resource, Ministry of Education; Yunnan Research & Development Center for Natural Products; School of Chemical Science and Technology, Yunnan University, Kunming 650091, P. R. China*

Quan Wang − *Yunnan Provincial Key Laboratory of Forensic Science, Yunnan Police College, Kunming 650223, P. R. China*

Ye-Ping Li − *Key Laboratory of Medicinal Chemistry for Natural Resource, Ministry of Education; Yunnan Research & Development Center for Natural Products; School of Chemical Science and Technology, Yunnan University, Kunming 650091, P. R. China*

Xiao Geng − *Key Laboratory of Medicinal Chemistry for Natural Resource, Ministry of Education; Yunnan Research & Development Center for Natural Products; School of Chemical Science and Technology, Yunnan University, Kunming 650091, P. R. China*

LiJia Zhao − *Key Laboratory of Medicinal Chemistry for Natural Resource, Ministry of Education; Yunnan Research & Development Center for Natural Products; School of Chemical Science and Technology, Yunnan University, Kunming 650091, P. R. China*

Mei He − *Key Laboratory of Medicinal Chemistry for Natural Resource, Ministry of Education; Yunnan Research & Development Center for Natural Products; School of Chemical Science and Technology, Yunnan University, Kunming 650091, P. R. China*

Complete contact information is available at: https://pubs.acs.org/10.1021/acsomega.1c00574

Author Contributions

[§]S.-F.L. and Q.W. contributed equally to this work.

Notes

The authors declare no competing financial interest.

■ ACKNOWLEDGMENTS

This work was supported by the National Natural Science Foundation of China (Nos. 21561033 and 22061047).

REFERENCES

(1) Vittal, J. J.; Quah, H. S. Engineering solid state structural transformations of metal complexes. *Coord. Chem. Rev.* **2017**, *342*, 1−18.

(2) Liu, Y.; O'Keeffe, M.; Treacy, M. M. J.; Yaghi, O. M. The geometry of periodic knots, polycatenanes and weaving from a chemical perspective: a library for reticular chemistry. *Chem. Soc. Rev.* **2018**, *47*, 4642−4664.

(3) Liu, J.; Pei, L.; Xia, Z.; Xu, Y. Hierarchical Accordion-like Lanthanide-Based Metal−Organic Frameworks: Solvent-Free Syntheses and Ratiometric Luminescence Temperature-Sensing Properties. *Cryst. Growth Des.* **2019**, *19*, 6586−6591.

(4) Wang, C.; Chai, L.; Luo, C.; Liu, S. Solvothermal preparation of nickel-iron phosphides hollow nanospheres derived from metal-organic frameworks for water oxidation reaction. *Appl. Surf. Sci.* **2021**, *540*, No. 148336.

(5) Wang, X.; Wang, X.; Zhang, X.; Fan, W.; Li, Q.; Jiang, W.; Dai, F.; Sun, D. A Stable Interpenetrated Zn-MOF with Efficient Light Hydrocarbon Adsorption/Separation Performance. *Cryst. Growth Des.* **2020**, *20*, 5670−5675.

(6) Reczyński, M.; Heczko, M.; Koziel, M.; Ohkoshi, S. I.; Sieklucka, B.; Nowicka, B. Proton-Conducting Humidity-Sensitive Ni(II)-Nb-(IV) Magnetic Coordination Network. *Inorg. Chem.* **2019**, *58*, 15812−15823.

(7) Liu, J.-L.; Chen, Y.-C.; Guo, F.-S.; Tong, M.-L. Recent advances in the design of magnetic molecules for use as cryogenic magnetic coolants. *Coord. Chem. Rev.* **2014**, *281*, 26−49.

(8) Zhou, L.; Zhao, M.; Zhang, X.; Zhang, J. Two Metal-Organic Frameworks Based on Hexanuclear Cobalt-Hydroxyl Clusters or a Manganese-Hydroxyl Chain from Triangular $[M^{II}_3(\mu_3\text{-OH})]$ (M = Co and Mn) Units: Antiferromagnetic and Spin-Canting Antiferromagnetic Ordering with Soft-Magnetic Behavior. *Inorg. Chem.* **2020**, *59*, 12017−12024.

(9) Kong, J.-J.; Jiang, Y.-X.; Zhang, J.-C.; Shao, D.; Huang, X.-C. Two-dimensional magnetic materials of cobalt(ii) triangular lattices constructed by a mixed benzimidazole−dicarboxylate strategy. *CrystEngComm* **2019**, *21*, 2596−2604.

(10) Son, K.; Kim, J. Y.; Schutz, G.; Kang, S. G.; Moon, H. R.; Oh, H. Coordinated Molecule-Modulated Magnetic Phase with Metamagnetism in Metal-Organic Frameworks. *Inorg. Chem.* **2019**, *58*, 8895−8899.

(11) Ghosh, S.; Ida, Y.; Ishida, T.; Ghosh, A. Linker Stoichiometry-Controlled Stepwise Supramolecular Growth of a Flexible Cu2Tb Single Molecule Magnet from Monomer to Dimer to One-Dimensional Chain. *Cryst. Growth Des.* **2014**, *14*, 2588−2598.

(12) Ma, Y.; Wen, Y. Q.; Zhang, J. Y.; Gao, E. Q.; Liu, C. M. Structures and magnetism of azide- and carboxylate-bridged metal(II) systems derived from 1,2-bis(N-carboxymethyl-4-pyridinio)ethane. *Dalton Trans.* **2010**, *39*, 1846−1854.

(13) Zhang, W.-X.; Xue, W.; Lin, J.-B.; Zheng, Y.-Z.; Chen, X.-M. 3D geometrically frustrated magnets assembled by transition metal ion and 1,2,3-triazole-4,5-dicarboxylate as triangular nodes. *CrystEngComm* **2008**, *10*, 1770−1776.

(14) Gao, W.; Huang, H.; Zhou, A.-M.; Wei, H.; Liu, J.-P.; Zhang, X.-M. Three 3D LnIII-MOFs based on a nitro-functionalized biphenyl-tricarboxylate ligand: syntheses, structures, and magnetic properties. *CrystEngComm* **2020**, *22*, 267−274.

(15) Zhao, S.-N.; Su, S.-Q.; Song, X.-Z.; Zhu, M.; Hao, Z.-M.; Meng, X.; Song, S.-Y.; Zhang, H.-J. A Series of Metal−Organic Frameworks Constructed From a V-shaped Tripodal Carboxylate Ligand: Syntheses, Structures, Photoluminescent, and Magnetic Properties. *Cryst. Growth Des.* **2013**, *13*, 2756−2765.

(16) Li, J.-J.; Wang, C.-C.; Guo, J.; Cui, J.-R.; Wang, P. Two zigzag chain-like lanthanide(III) coordination polymers based on the rigid 1,3-adamantanedicarboxylic acid ligand: Crystal structure, luminescence and magnetic properties. *Polyhedron* **2017**, *126*, 17−22.

(17) Sran, B. S.; Sharma, S.; Pointillart, F.; Cador, O.; Hundal, G. Field-Induced Single Molecular Magnetism and Photoluminescence in Rare Cocrystals of Isomorphic Lanthanide(III) Coordination Compounds with Fully Substituted Pyridine-4-carboxamide Ligand. *Inorg. Chem.* **2020**, *59*, 9227−9238.

(18) Zhu, Q.; Sheng, T.; Fu, R.; Hu, S.; Shen, C.; Ma, X.; Wu, X. Syntheses, structural aspects, luminescence and magnetism of four coordination polymers based on a new flexible polycarboxylate. *CrystEngComm* **2011**, *13*, 2096−2105.

(19) Liu, X.; Du, L.; Wang, Y.; Li, R.; Feng, X.; Ding, Y. Synthesis, crystal structures and properties of two nickel (II) complexes with different nitrogen-heterocyclic polycarboxylate ligand. *J. Mol. Struct.* **2019**, *1186*, 224−229.

(20) Zhang, C.; Ma, X.; Cen, P.; Jin, X.; Yang, J.; Zhang, Y. Q.; Ferrando-Soria, J.; Pardo, E.; Liu, X. A series of lanthanide(III) metal-organic frameworks derived from a pyridyl-dicarboxylate ligand: single-molecule magnet behaviour and luminescence properties. *Dalton Trans.* **2020**, *49*, 14123−14132.

(21) Wang, C.-C.; Wang, J.-H.; Tang, G.-M.; Wang, Y.-T.; Cui, Y.-Z.; Ng, S. W. Syntheses, crystal structures, and luminescent properties of three metal coordination polymers based on adipic acid and 2-(pyridine-3-yl)-(1H)-benzimidazole. *J. Coord. Chem.* **2015**, *68*, 3918−3931.

(22) Xie, X.; Zhang, Z.; Zhang, J.; Hou, L.; Li, Z.; Li, G. Impressive Proton Conductivities of Two Highly Stable Metal-Organic Frameworks Constructed by Substituted Imidazoledicarboxylates. *Inorg. Chem.* **2019**, *58*, 5173−5182.

(23) Qin, Y.; Li, Y.; Guo, K.; Tang, H.; Hou, L.; Li, G. Water-assisted proton conductivity of two highly stable imidazole multi-carboxylate-based MOFs. *New J. Chem.* **2019**, *43*, 4859−4866.

(24) Feng, J.; Yu, S.; Guo, K.; Li, J.; Li, G. Water-mediated proton conduction for a highly stable strontium-organic framework from imidazole multi-carboxylate ligand. *Polyhedron* **2019**, *169*, 1−7.

(25) Liang, X.; Li, B.; Wang, M.; Wang, J.; Liu, R.; Li, G. Effective Approach to Promoting the Proton Conductivity of Metal-Organic Frameworks by Exposure to Aqua-Ammonia Vapor. *ACS Appl. Mater. Interfaces* **2017**, *9*, 25082−25086.

(26) Hübner, W.; Pavlyukh, Y.; Lefkidis, G.; Berakdar, J. Magnetism of a four-center transition-metal cluster revisited. *Phys. Rev. B* **2017**, *96*, No. 184432.

(27) Huttner, G.; Lorenz, H. Die Struktur des Nickel-Clusters $H_3(C_5H_5)_4Ni_4$. *Chem. Ber.* **1974**, *107*, 996−1008.

(28) Karmakar, T. K.; Chandra, S. K.; Ribas, J.; Mostafa, G.; Lu, T. H.; Ghosh, B. K. Synthesis, structure and magnetism of a new dicubane-like ferromagnetic tetranuclear nickel cluster containing versatile azido-only bridges and a bis(bidentate) Schiff base blocker. *Chem. Commun.* **2002**, 2364−2365.

(29) King, P.; Clerac, R.; Wernsdorfer, W.; Anson, C. E.; Powell, A. K. Synthesis and magnetism of oxygen-bridged tetranuclear defect dicubane Co(II) and Ni(II) clusters. *Dalton Trans.* **2004**, 2670−2676.

(30) Chilton, N. F.; Anderson, R. P.; Turner, L. D.; Soncini, A.; Murray, K. S. PHI: a powerful new program for the analysis of anisotropic monomeric and exchange-coupled polynuclear d- and f-block complexes. *J. Comput. Chem.* **2013**, *34*, 1164−1175.

(31) Zhao, F.-H.; Li, Z.-L.; He, Y.-C.; Huang, L.-W.; Jia, X.-M.; Yan, X.-Q.; Wang, Y.-F.; You, J.-M. 1D Water cages in a double-walled framework based on cubic $[Ni_4(\mu_3\text{-OH})_4]$ units: Synthesis, structure, and magnetism. *J. Solid State Chem.* **2019**, *271*, 309−313.

(32) Jing, X.-H.; Yi, X.-C.; Gao, E.-Q.; Blatov, V. A. Synthesis, structure, topology and magnetic properties of cobalt(ii) coordination polymers with 2-nitrobiphenyl-4,4′-dicarboxylic acid and bis(pyridyl) ligands. *Dalton Trans.* **2012**, *41*, 14316−14328.

(33) Reuse, F. A.; Khanna, S. N. Geometry, electronic structure, and magnetism of small Nin (n = 2−6, 8, 13) clusters. *Chem. Phys. Lett.* **1995**, *234*, 77−81.

(34) Vreugdenhill, W.; Haasnoot, J. G.; Reedijk, J.; Spek, A. L. Ferromagnetic and antiferromagnetic spin coupling in Ni4O4 cubane-type clusters with 4-amino-3,5-bis(hydroxymethyl)-1,2,4-triazole as a ligand. The x-ray structure of a new dumbbell-like double cubane cluster. *Inorg. Chim. Acta* **1987**, *129*, 205−216.

(35) Wang, S.; Wang, W.; Li, H.; Xing, Y.; Hou, K.; Li, H. Rapid On-Site Detection of Illegal Drugs in Complex Matrix by Thermal

https://doi.org/10.1021/acsomega.1c00574
ACS Omega 2021, 6, 9213−9221

Desorption Acetone-Assisted Photoionization Miniature Ion Trap Mass Spectrometer. *Anal. Chem.* **2019**, *91*, 3845−3851.
(36) Myers, B.; Berger, L.; Friedberg, S. Low-Temperature Magnetization of $Cu(NO_3)_2{\cdot}2.5H_2O$. *J. Appl. Phys.* **1969**, *40*, 1149−1151.
(37) O'Connor, C. J.; Klein, C. L.; Majeste, R. J.; Trefonas, L. M. Magnetic properties and crystal structure of (2, 3-pyrazinedicarboxylato) copper (II) hydrochloride: a pyrazine bridged ferromagnetic linear chain. *Inorg. Chem.* **1982**, *21*, 64−67.
(38) King, P.; Clérac, R.; Wernsdorfer, W.; Anson, C. E.; Powell, A. K. Synthesis and magnetism of oxygen-bridged tetranuclear defect dicubane Co (II) and Ni (II) clusters. *Dalton Trans.* **2004**, 2670−2676.
(39) Yamada, T.; Nankawa, T. High Proton Conductivity of Zinc Oxalate Coordination Polymers Mediated by a Hydrogen Bond with Pyridinium. *Inorg. Chem.* **2016**, *55*, 8267−8670.
(40) Moi, R.; Ghorai, A.; Banerjee, S.; Biradha, K. Amino- and Sulfonate-Functionalized Metal−Organic Framework for Fabrication of Proton Exchange Membranes with Improved Proton Conductivity. *Cryst. Growth Des.* **2020**, *20*, 5557−5563.
(41) Xing, X. S.; Fu, Z. H.; Zhang, N. N.; Yu, X. Q.; Wang, M. S.; Guo, G. C. High proton conduction in an excellent water-stable gadolinium metal-organic framework. *Chem. Commun.* **2019**, *55*, 1241−1244.
(42) Qin, Y.; Xue, M.-H.; Dou, B.-H.; Sun, Z.-B.; Li, G. High protonic conduction in two metal−organic frameworks containing high-density carboxylic groups. *New J. Chem.* **2020**, *44*, 2741−2748.
(43) Kreuer, K.-D.; Rabenau, A.; Weppner, W. Vehicle Mechanism, A New Model for the Interpretation of the Conductivity of Fast Proton Conductors, 1982.
(44) Kreuer, K.-D. Proton Conductivity: Materials and Applications. *Chem. Mater.* **1996**, *8*, 610−641.
(45) Agmon, N. The Grotthuss mechanism. *Chem. Phys. Lett.* **1995**, *244*, 456−462.
(46) Sheldrick, G. M. J. S. *SADABS: Program for Empirical Absorption Correction of Area Detector Data*, 1996.
(47) Sheldrick, G. Crystal structure refinement with SHELXL. *Acta Crystallogr., Sect. C* **2015**, *71*, 3−8.
(48) Spek, A. Structure validation in chemical crystallography. *Acta Crystallogr., Sect. D* **2009**, *65*, 148−155.

https://doi.org/10.1021/acsomega.1c00574
ACS Omega 2021, 6, 9213−9221